INTERNATIONAL JOURNAL FOR NUMERICAL METHODS IN FLUIDS
Int. J. Numer. Meth. Fluids 2003; **42**:791–812 (DOI: 10.1002/fld.554)

A new VOF-based numerical scheme for the simulation of fluid flow with free surface. Part II: application to the cavity filling and sloshing problems

Min Soo Kim[1], Jong Sun Park[2] and Woo Il Lee[2,*,†]

[1]*MEMS Lab, Samsung Advanced Institute of Technology, P.O. Box 111, Suwon 440-600, Korea*
[2]*School of Mechanical and Aerospace Engineering, Seoul National University, Seoul 151-742, Korea*

SUMMARY

Finite element analysis of fluid flow with moving free surface has been performed in 2-D and 3-D. The new VOF-based numerical algorithm that has been proposed by the present authors (Int. J. Numer. Meth. Fluids, submitted) was applied to several 2-D and 3-D free surface flow problems. The proposed free surface tracking scheme is based on two numerical tools; the orientation vector to represent the free surface orientation in each cell and the baby-cell to determine the fluid volume flux at each cell boundary. The proposed numerical algorithm has been applied to 2-D and 3-D cavity filling and sloshing problems in order to demonstrate the versatility and effectiveness of the scheme. The proposed numerical algorithm resolved successfully the free surfaces interacting with each other. The simulated results demonstrated applicability of the proposed numerical algorithm to the practical problems of large free surface motion. It has been also demonstrated that the proposed free surface tracking scheme can be easily implemented in any irregular non-uniform grid systems and can be extended to 3-D free surface flow problems without additional efforts. Copyright © 2003 John Wiley & Sons, Ltd.

KEY WORDS: free surface; volume of fluid (VOF) method; orientation vector; baby-cell; cavity filling problem; sloshing problem

1. INTRODUCTION

Fluid flow with moving free surface has many engineering applications. Examples include manufacturing processes such as metal and glass forming, injection and compression molding of polymeric resins, crystal growth, and so on. Since the fluid flow implies many physical aspects in such processes, a throughout analysis using a proper method is necessary. However, difficulties arise from the fact that the domain of interest has unknown boundary that should

*Correspondence to: W. I. Lee, School of Mechanical and Aerospace Engineering, Seoul National University, San 56-1, Shilim-dong, Kwanak-ku, Seoul 151-742, Korea.
†E-mail: wilee@snu.ac.kr

Contract/grant sponsor: Brain Korea-21 Project
Contract/grant sponsor: Korea Ministry of Science and Technology

Received 3 November 2000
Revised 11 March 2003

be determined as a part of the solution. To treat free surface numerically, it is required to adopt an accurate and efficient scheme that can resolve the free surface moving continuously with time. Being faithful to the physical phenomena on the moving free surface, the scheme should be able to depict actual free surface configurations. In addition to simple structure, the scheme should be equipped with extensibility to 3-D free surface flow problems.

With these requirements satisfied, a new free surface tracking scheme based on the VOF method [1] has been proposed by the present authors [2, 3]. The proposed free surface tracking scheme can trace the free surface with minimal numerical smearing. Also, the scheme was devised so that it can be applied to 3-D problems without additional efforts and can be implemented in irregular non-uniform grid systems. Novel features of the proposed scheme are characterized by two numerical tools. One is the orientation vector to represent the free surface orientation in each cell and the other is the baby-cell to determine the fluid volume flux at each cell boundary [2]. Efficiency of the proposed numerical algorithm as well as its accuracy in tracking of free surface has been demonstrated through simulation of broken dam and solitary wave propagation problems [2].

Cavity filling and sloshing are typical free surface flow problems that accompany large deformation of free surface. Cavity filling is commonly encountered in the manufacturing or forming processes where molten metal or polymeric resin is injected into the mold cavity, then solidified and separated. Analyses of cavity filling problems have been done through various methods by many researchers. In general, due to complex shape of mold cavity, most analyses have been based on fixed grid systems. Especially, many analyses have resorted to the VOF method [4–15]. Dhatt *et al.* [4] simulated two-dimensional casting processes using the penalty method and Taylor–Galerkin formulation. They applied the shear stress boundary condition using a wall function. Chan *et al.* [5], Minaie *et al.* [6], Usmani *et al.* [7] and Rice [8] carried out filling and heat transfer analyses in the die casting process. Among them, Usmani *et al.* [7] and Lewis *et al.* [9] analysed the two-dimensional casting processes using Taylor–Galerkin formulation with the solution of pseudo-concentration transport equation. Hetu and Ilinica [10] analysed the mold filling and solidification processes using the level-set method and adopted a mixing length turbulence model. They applied the boundary condition of surface traction and used a Chezy law for surface traction. Gao [11] analysed three-dimensional mould filling processes using the mixed formulation and a PLIC-type free surface representation. Gao applied an unstructured element (P1+/P1) and adopted a zero equation model for turbulence. On the other hand, some researchers applied the turbulence model, usually, k–ε model to casting processes [12, 13]. Swaminathan and Voller [14] have presented a 'time-implicit filling algorithm' while Shin and Lee [15] have presented a selective VOF method and analysed cavity filling under the effect of gravity. However, many analyses were limited to the case of simple filling where mold cavity is filled with the fluid advancing unidirectionally and free surface advances with configuration nearly perpendicular to the flow direction (i.e. filling direction). In most cases, free surface location was traced approximately. Therefore, large deformation of free surface, especially 3-D cavity filling problems could not be dealt with accurately.

Sloshing is a liquid motion with free surface in a container. Analysis of fluid motion is necessary to prevent detrimental situations such as overflow of fluid or overturn of structure during fluid–structure interactions. In a number of numerical studies, Lagrangian method such as Lagrangian FEM [16, 17] or ALE method [18, 19] has been adopted to describe free surface motion. Ramaswamy *et al.* [16] and Okamoto and Kawahara [17] analysed 2-D sloshing

motion using Lagrangian FEM. However, in Lagrangian methods, it was impossible to simulate the free surface undergoing large deformation or moving abruptly. On the other hand, using VOF method, Partom [20] simulated sloshing motion in a partially filled cylindrical container. Jun and Spalding [21] also employed VOF method for 2-D analysis. However, most sloshing analyses were limited to 2-D problems. Besides, numerical smearing on the moving free surface was present.

In this article, the new free surface tracking algorithm that has been proposed by the present authors [2] was applied to 2-D and 3-D cavity filling and sloshing problems. The simulated results demonstrated versatility and effectiveness of the new free surface tracking scheme as well as the overall solution algorithm.

2. CAVITY FILLING PROBLEMS

In this section, the numerical simulation was done for 2-D and 3-D cavity filling problems. The algorithm for the calculation is based on the new free surface tracking scheme that has been proposed by the present authors [2]. Also, the simulated results were compared with the results obtained using commercial CFD package FLOW-3D® that has been widely used in the simulation of various free surface flow problems. In the following simulations, the number of baby-cells was chosen as 1600 ($=40\times40$) in 2-D and 1000 ($=10\times10\times10$) in 3-D. Although the effects of the number of baby-cells on the accuracy of solution were not investigated in this study, simple consideration shows that the maximum error in the estimated wet-out fraction is 2.5% ($=1/40$) for 1600 baby-cells in 2-D and 1% ($=1/10\times10$) for 1000 baby-cells in 3-D. Therefore, the number of baby-cells chosen in the present study is reasonable from a consideration that the overall accuracy in the numerical solution of free surface fluid flow is influenced by the computational accuracy of the flow field (especially, pressure field), time integration method of the transport equation of f, determination of free surface orientation in a cell and the size of time increment.

2.1. 2-D cavity filling problem

Filling of 2-D mold cavity under the effect of gravity has been simulated. Definition of the problem is illustrated in Figure 1(a). Mold cavity is a square ($L\times L,\ L=0.4\,\mathrm{m}$). Inlet of the cavity is located in the middle of upper wall and is one third of cavity dimension ($d=L/3$). Density and viscosity of the fluid are $1000\,\mathrm{kg/m^3}$ and 1 Pa.s, respectively. The ambient fluid is air. The acceleration of gravity is $g=9.8\,\mathrm{m/s^2}$ and acts in downward direction. Initially the inlet of mold cavity was assumed to be filled with a small amount of fluid ($d\times l,\ l=L/10$) such that the initial filled fraction of the cavity is 3.33%. The mesh used is composed of uniform 21×21 grids, which has 400 finite elements and 441 nodes (see Figure 1(b)). A parabolic velocity distribution was assumed at the inlet with an average velocity of $V_{\mathrm{avg}}=1\mathrm{m/s}$.

No-slip boundary conditions at the wall would lead to a very sluggish and unrealistic flow. This is because the relatively coarse mesh used in this study cannot effectively resolve the thin boundary layer at the wall. This problem can be remedied by allowing the fluid to slip at the wall with some surface traction. In this simulation, therefore, slip boundary conditions were assumed on the wall, where the surface traction was modeled as an equivalent volume force [3, 22].

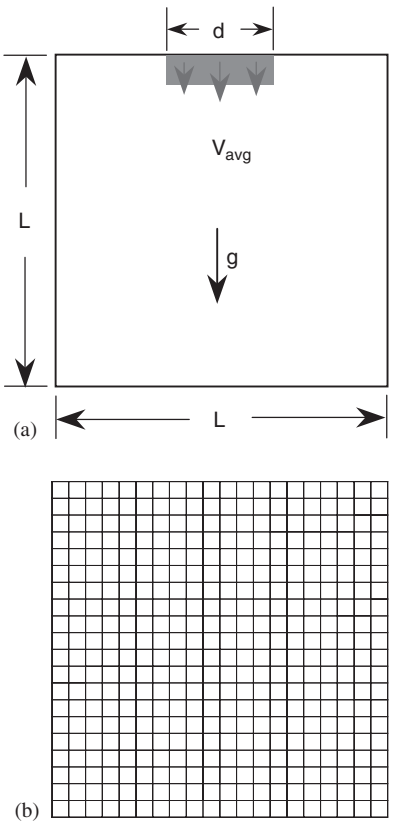

Figure 1. Definition sketch for 2-D cavity filling. (a) Square mold cavity and (b) a uniform 21×21 mesh.

In order to approximate tangential tractions at the mold wall in simulations of metal casting, Usmani *et al.* [7] and Lewis *et al.* [9] used von Karman's law of the wall, which has been usually applied to the turbulent flow problems. Rice [8] evaluated the surface traction in an explicit manner from the previous iteration in the mold filling analysis. In RIPPLE program [22], on the other hand, surface force (e.g. surface tension effect) was modelled as body force acting on the elements that is lying within a finite thickness transition region. In a similar manner, in the present study, unknown surface traction on the wall was modeled as volume force acting on the element adjacent to the wall boundary. Surface traction term in FE formulation of momentum equations can be reshaped into an equivalent body force term as follows [3]:

$$\frac{1}{\rho}\,\bar{t}_i\,\mathrm{d}A \sim \left(\frac{1}{\rho}\,\bar{t}_i\,\frac{1}{\delta}\right)\mathrm{d}V \sim f_i^t\,\mathrm{d}V \tag{1}$$

where $\bar{t}_i$ denotes the surface traction on the wall and δ denotes the boundary layer thickness. $\mathrm{d}A$ and $\mathrm{d}V$ are the infinitesimal area and volume elements on the wall, respectively. f_i^t represents the equivalent body force per unit volume acting in the ith co-ordinate direction.

The surface traction $\bar{t}_i$ and the boundary layer thickness δ can be approximated using, for example, expressions for the laminar boundary layer on a flat plate [23].

$$\bar{t}_i \approx \frac{\rho |u_i^{\mathrm{w}}|^2}{\sqrt{Re}} \quad \text{and} \quad \delta \approx \frac{L_{\mathrm{c}}}{\sqrt{Re}} \tag{2}$$

where Re is the Reynolds number, u_i^{w} denotes the ith component of tangential velocity on the wall and L_{c} represents the characteristic length of the problem considered. Thus, the equivalent body force can be approximated from the information on the previous tangential velocity on the wall as

$$f_i^t = -C \frac{|u_i^{\mathrm{w}}| u_i^{\mathrm{w}}}{L_{\mathrm{c}}} \tag{3}$$

where C is the positive coefficient depending on the expressions adopted for $\bar{t}_i$ and δ. In the present study, L_{c} was chosen as the size of the inlet [3].

In Figure 2, calculated configurations of free surface are shown together with velocity vector fields. The calculated results were plotted for time interval of $\Delta t = 0.08$ s. Due to the gravity effect, fluid accelerates as it enters the cavity. Fluid reaches the bottom wall and splits to both sides. With some inertia, fluid climbs the vertical walls, then is pulled down by gravity and collides with the incoming fluid stream near the centre of cavity. When two free surfaces merge together, another free surface is created and it diminishes gradually by subsequent filling of fluid. Thereafter, the cavity is filled with the fluid having nearly horizontal free surface.

As experimental data are not available for comparison, the same problem was solved using the commercial CFD package FLOW-3D®, which has been widely used in the simulation of various free surface flow problems. In FLOW-3D®, movement of free surface is modelled by the original VOF method [1] with some improvements in the advection treatment. Solution algorithm is based on the finite difference control volume method, and no-slip boundary conditions are assumed on the wall. In Figure 3, the free surface configurations predicted by FLOW-3D® are shown together with velocity vector fields. Overall filling patterns are similar to those obtained with the present scheme. However, a slight difference is observed at the wall. Flow is excessively retarded at the wall, resulting in an unrealistic movement of the free surface. The wall boundary layer seemed to be overestimated due to the no-slip boundary conditions enforced with relatively coarse grids. On the other hand, the fill time based on the inlet condition is 1.16 s. The fill time predicted by the present scheme was 1.150 s, whereas with FLOW-3D® was 1.122 s: Fill time errors were 0.86 and 3.27% for the present scheme and the FLOW-3D®, respectively. These comparisons show that the proposed solution algorithm could simulate the dynamics in filling of mold cavity with a realistic behaviour as well as with a negligible mass loss.

2.2. 3-D cavity filling problem

Filling of 3-D mold cavity under the effect of gravity has been considered. Definition of the problem is illustrated in Figure 4(a). Mold cavity is a square column ($0.2\,\mathrm{m} \times 0.2\,\mathrm{m} \times 0.4\,\mathrm{m}$). Inlet of the cavity is a circle of which diameter is $d = a/2$. Calculations were carried out for two mold cavities of different inlet locations (see Figure 4(b)). Inlet is located either at the centre of upper wall ($e_x = 0$, $e_y = 0$) or slightly shifted from the centre of upper wall ($e_x = 0.1a$,

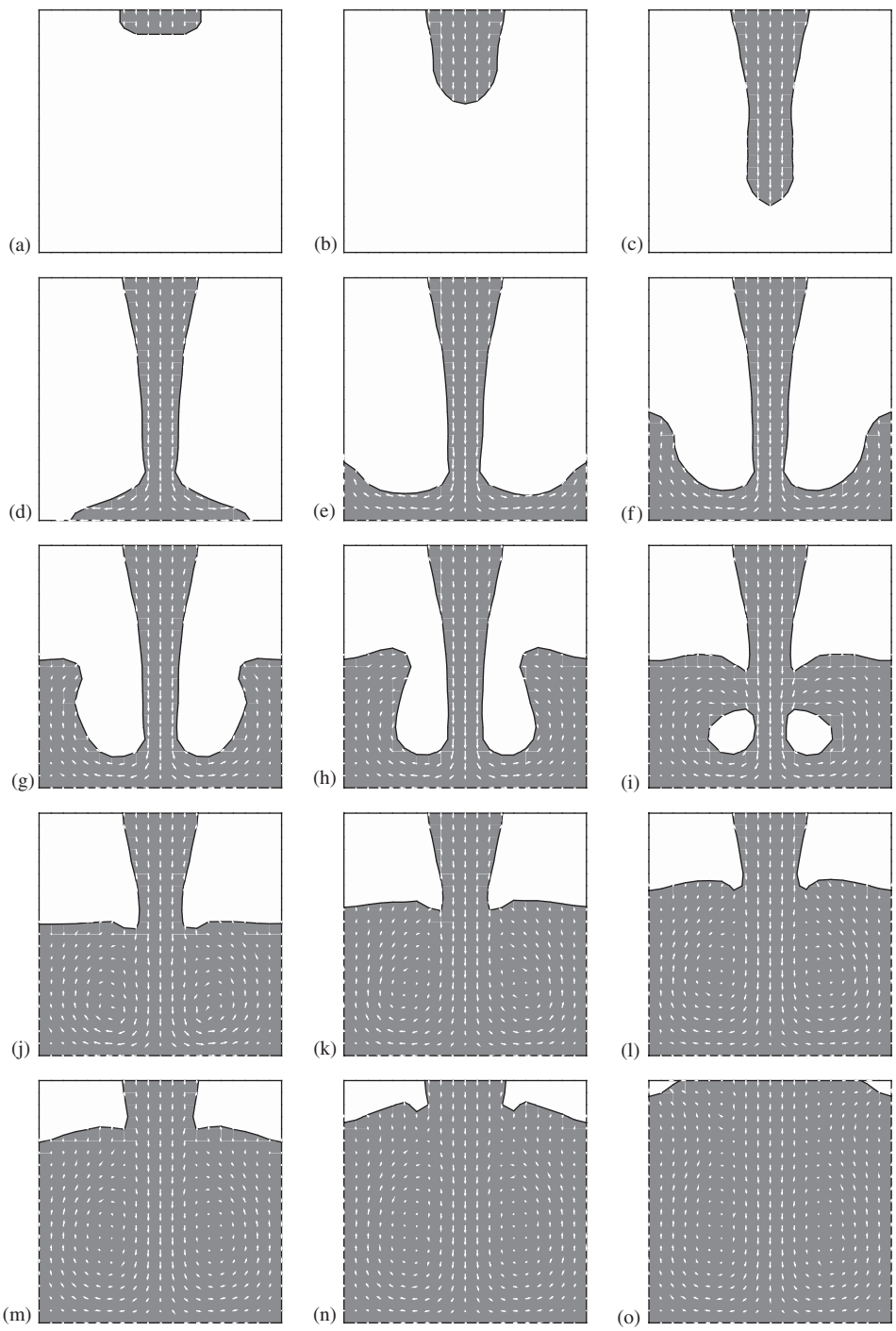

Figure 2. Free surface profiles and velocity vectors in 2-D cavity filling. Results obtained with the present numerical scheme. Time increment is $\Delta t = 0.08$ s.

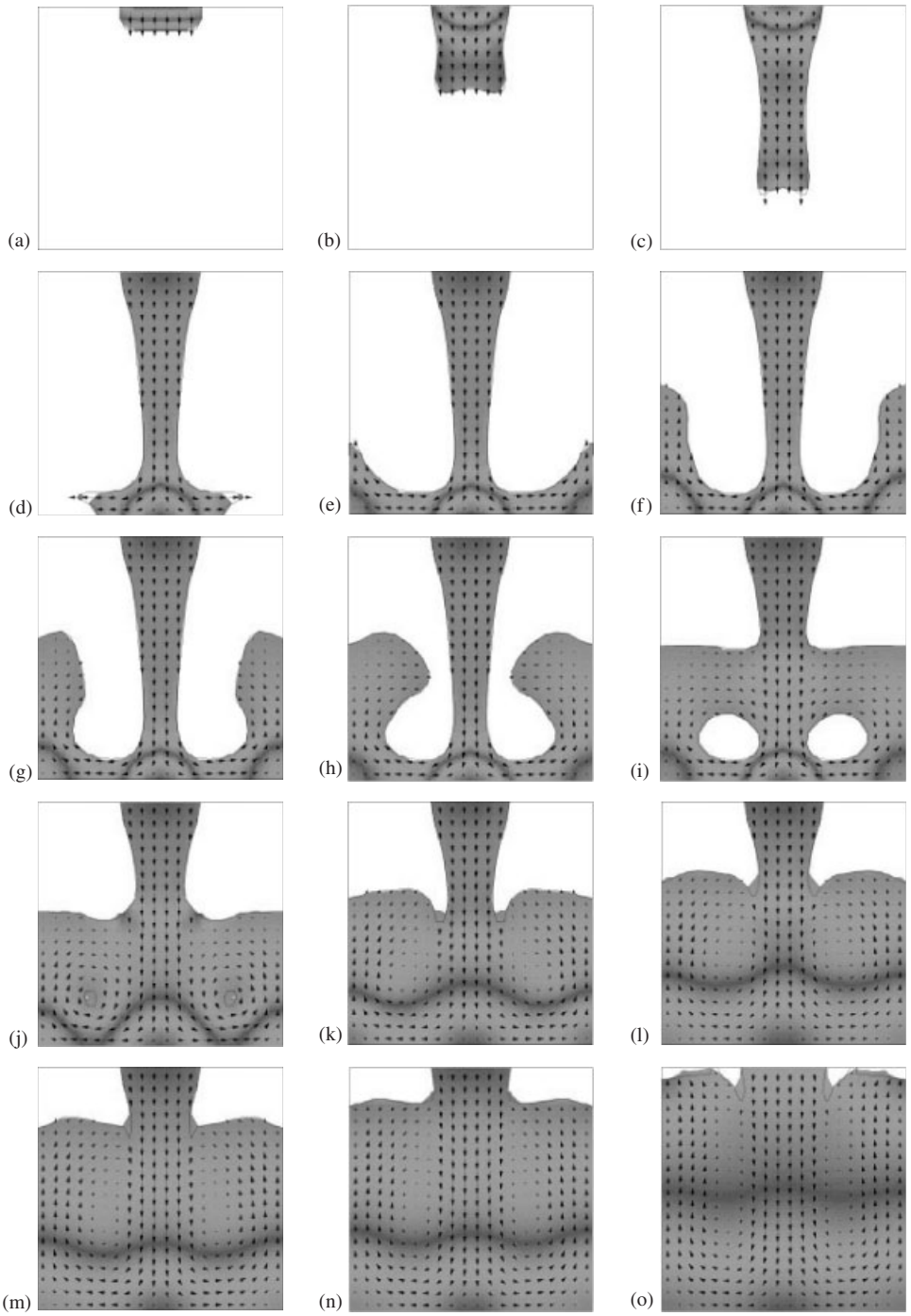

Figure 3. Free surface profiles and velocity vectors in 2-D cavity filling. Results obtained with FLOW-3D®. Time increment is $\Delta t = 0.08$ s.

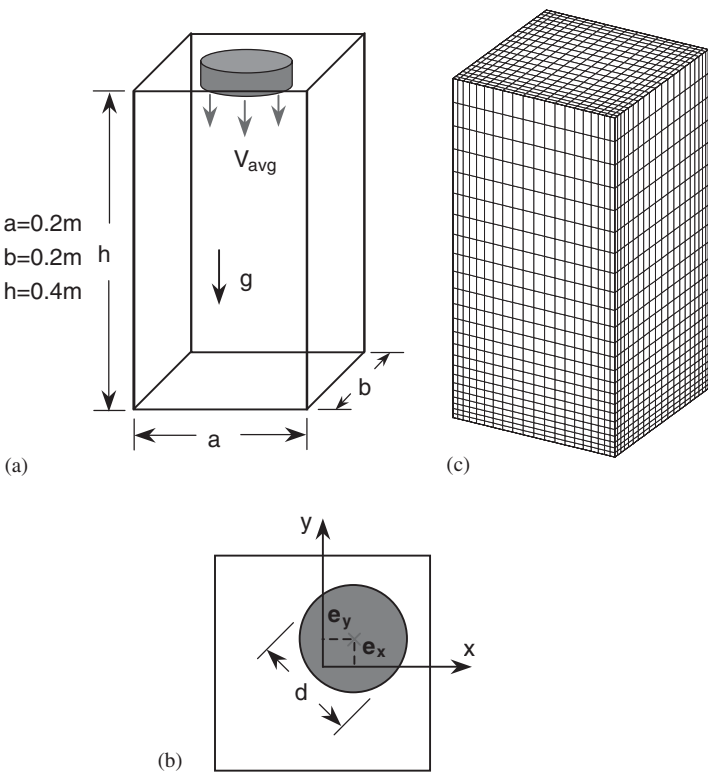

Figure 4. Definition sketch for 3-D cavity filling. (a) mold cavity, (b) cavity inlet, and (c) a $21 \times 21 \times 25$ mesh used in the numerical simulation.

$e_y = 0.05b$). Properties of the fluid are same as the previous example ($\rho = 1000\ \mathrm{kg/m^3}$ and $\mu = 1$ Pa.s). The ambient fluid is air. The acceleration of gravity is $g = 9.8\ \mathrm{m/s^2}$ and acts downward. Initially the inlet of mold cavity is filled with a small amount of fluid such that the initial filled fraction of the cavity is 3.0%. The mesh used is composed of non-uniform $21 \times 21 \times 25$ grids, which has 9600 finite elements and 11 025 nodes (see Figure 4(c)). A paraboloidal velocity distribution was assumed at the inlet with average velocity of $V_{\mathrm{avg}} = 1\mathrm{m/s}$. On the wall, slip boundary conditions were assumed with the surface traction modeled as an equivalent volume force [3, 22].

For the case of centred injection hole, evolution of free surface profiles is shown in Figure 5. Fluid accelerates due to the gravity effect as it enters the cavity and the fluid column becomes slender as it approaches the bottom wall. As fluid reaches the bottom, it spreads out in radial direction. Free surface reaches four surrounding vertical walls and subsequently four corners. Fluid climbs up rapidly along the walls with large inertia at first but is pulled down by the gravity. The descending fluid collides with incoming fluid stream in the lower part of the cavity. Two free surfaces merge together, creating another free surface inside the fluid region. The new free surface fades away by subsequent filling of the fluid. Thereafter, the cavity becomes filled with the fluid of nearly horizontal free surface. As the cavity becomes filled up, the winding free surface is smoothed out.

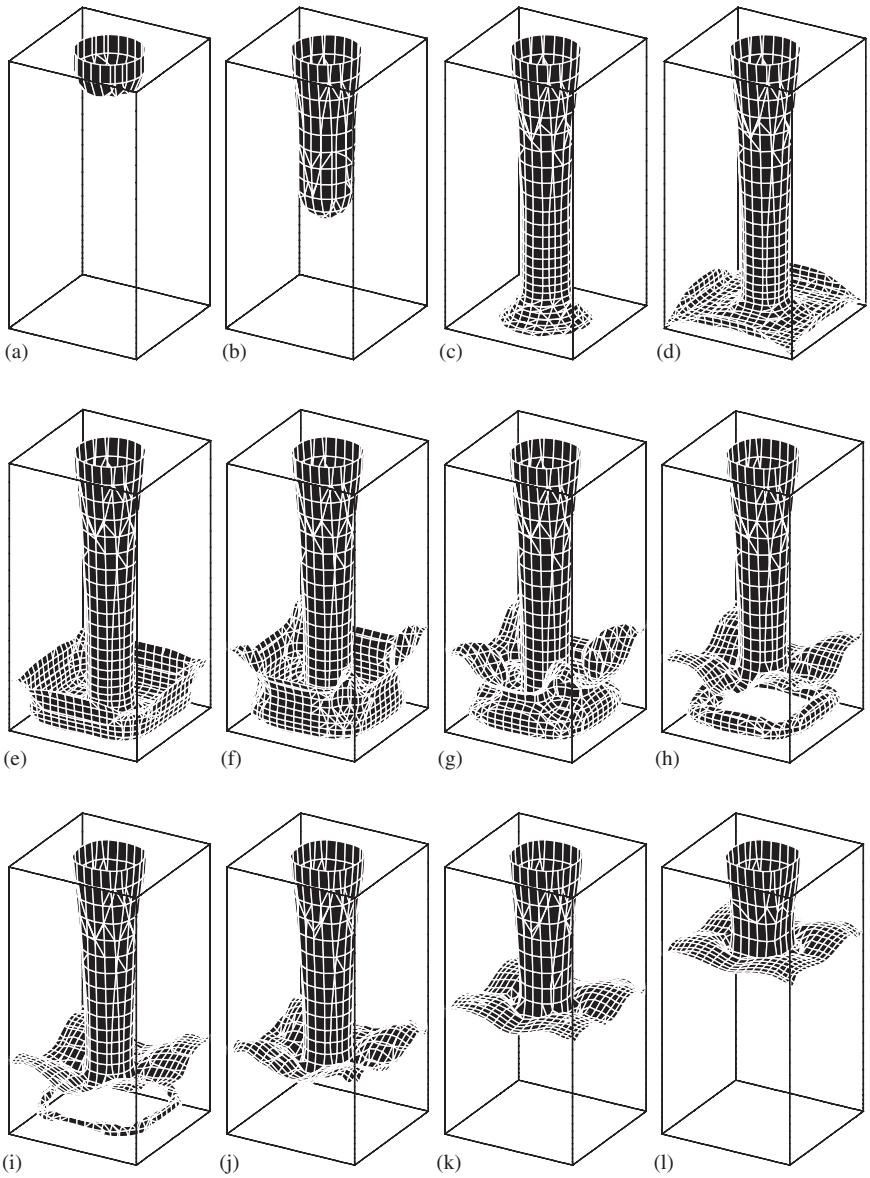

Figure 5. Free surface profiles during filling of 3-D cavity with a centred injection hole. Results obtained with the present numerical scheme. (a) 0 s, (b) 0.12 s, (c) 0.20 s, (d) 0.24 s, (e) 0.28 s, (f) 0.36 s, (g) 0.44 s, (h) 0.52 s, (i) 0.56 s, (j) 0.68 s, (k) 1.00 s, and (l) 1.40 s.

The same problem was simulated using FLOW-3D® for comparison and the calculated results are shown in Figure 6. Overall filling patterns from FLOW-3D® resemble those obtained with the present scheme. Here, as experienced in the 2-D simulation, flow is excessively retarded at the wall, especially at the corners. The wall boundary layer seemed to be

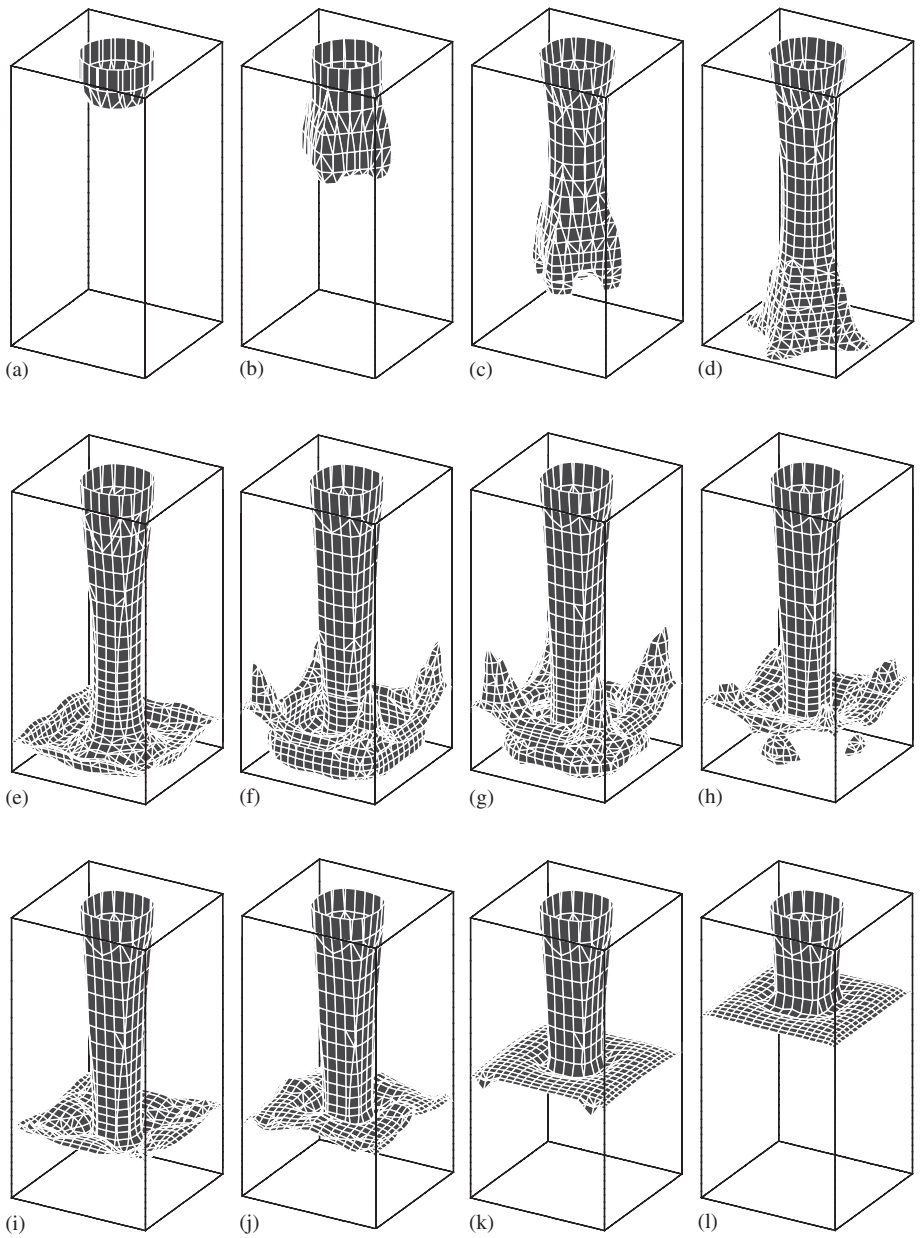

Figure 6. Free surface profiles during filling of 3-D cavity with a centred injection hole. Results obtained with FLOW-3D®. (a) 0 s, (b) 0.12 s, (c) 0.20 s, (d) 0.24 s, (e) 0.28 s, (f) 0.36 s, (g) 0.44 s, (h) 0.52 s, (i) 0.56 s, (j) 0.68 s, (k) 1.00 s, and (l) 1.40 s.

overestimated due to the no-slip boundary conditions enforced on the wall, where relatively coarse grids were used. In Figure 6, the fluid that has travelled up along the wall does not move far toward the incoming fluid stream due to big loss of inertia. Instead, it falls almost

vertically, resulting in a smaller new free surface inside fluid region. Furthermore, the free surface becomes unrealistically flat right after the new free surface disappears by subsequent filling of the fluid. A possible reason for this might be that the no-slip effect on the wall propagated rapidly toward the centre of the cavity.

Evolution of free surface profiles for the case of off-centred injection hole is shown in Figure 7. Fluid accelerates as it enters the cavity. Fluid first climbs up along the closer wall, resulting in different run-up heights at each corner. The asymmetric filling pattern is clearly seen in Figure 7. Subsequent fluid motion is much larger than that in the case of the centred injection hole, but the motion becomes smaller as the cavity is filled up.

3. SLOSHING PROBLEMS

Sloshing is a liquid motion with free surface in a container and has an engineering significance. During fluid–structure interactions, sloshing motion may cause detrimental effects such as overflow of fluid or overturn of structures. Analysis of sloshing motion is also very important, for instance, in the seismic problems associated with large fuel storage tanks or nuclear reactor systems. Other examples include the oil tankers during sailing and the fuel tanks of aircrafts or spacecrafts. A number of numerical studies have been performed. However, in most studies adopting the Lagrangian method for the description of free surface motion [16–19], free surfaces undergoing large deformation could not be simulated effectively. In the analyses using VOF method [20, 21], numerical smearing on the free surface was not suppressed effectively and 3-D sloshing problems could not be simulated accurately. In this section, 2-D and 3-D sloshing problems have been simulated using the proposed numerical scheme, and the robustness of the proposed numerical algorithm has been demonstrated.

A sloshing motion is usually created by movement of a container. Therefore, it is convenient to use a co-ordinate system fixed to the container. In the present sloshing simulations, a non-inertial co-ordinate system has been adopted [24]. Both the liquid and air were treated as incompressible fluids with physical properties at standard conditions.

3.1. 2-D forced sinusoidal horizontal oscillation

As seen in Figure 8(a), a container that is partially filled with water is at rest initially and then is forced to move horizontally in a sinusoidal manner. Dimensions of the container were chosen equal to those in the experiment of Okamoto and Kawahara [17] (see Figure 8(a)). They also have carried out a numerical simulation using Lagrangian FEM. Displacement of the container is given as $D = A\sin(\omega t)$, where A and ω denote the amplitude and the frequency of forced oscillation, respectively. In the present calculation, the amplitude A and the period $T(=1/\omega)$ were selected as 0.93 cm and 1.183 s, respectively. This value of period corresponds to the resonance frequency, as will be shown later. Initial depth of liquid, d, is 0.5 m. Frictionless boundaries were assumed between the fluid and the wall. The numerical mesh consists of non-uniform 41×49 grids, where the numbers of nodes and finite elements are 2009 and 1920, respectively (see Figure 8(b)).

Figure 9 shows the calculated free surface profiles. Sloshing motion is weak in earlier stage, but it becomes larger as time elapses. After a certain maximum height is reached, the sloshing motion dwindles down and then grows larger again. This repeated behaviour is

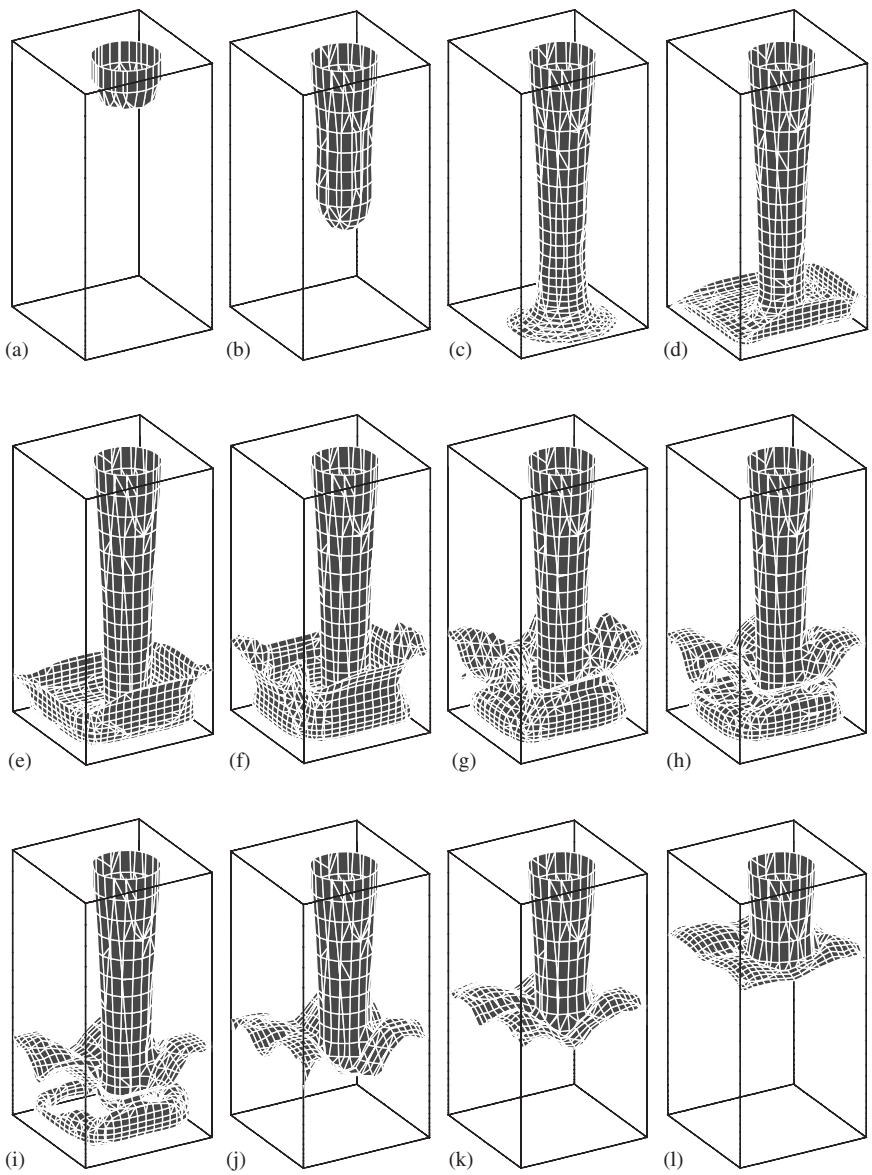

Figure 7. Free surface profiles during filling of 3-D cavity with an off-centred injection hole. Results obtained with the present numerical scheme. (a) 0 s, (b) 0.12 s, (c) 0.20 s, (d) 0.24 s, (e) 0.28 s, (f) 0.36 s, (g) 0.44 s, (h) 0.52 s, (i) 0.56 s, (j) 0.80 s, (k) 1.00 s, and (l) 1.40 s.

clearly seen in Figure 10, where the time histories of wave height at the vertical walls are given. Both the wave heights at two opposite walls have phase lag of a half cycle, and the upward displacement is almost twice the downward displacement. The results obtained with the present numerical scheme were in qualitative agreement with the experimental and numerical

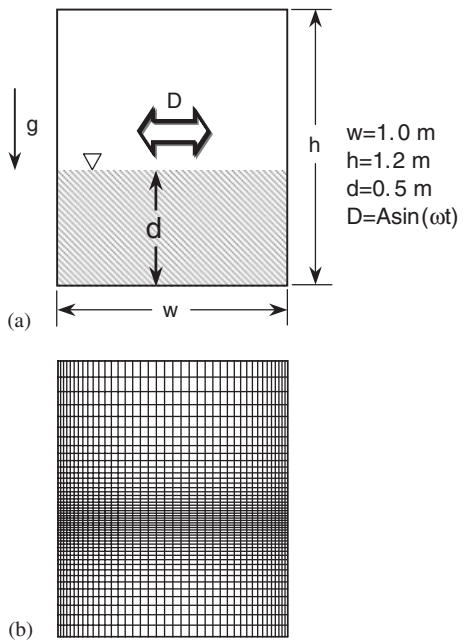

Figure 8. Definition sketch for sloshing in a container subject to forced sinusoidal horizontal oscillation. (a) Container partially filled with water and (b) a non-uniform 41×49 mesh.

results by Okamoto and Kawahara [17]. However, since their results were limited to the initial small amplitude sloshing motion, quantitative comparison was not available. Figure 11 depicts the variation of maximum wave height at the wall for several selected frequencies. It is confirmed that the period used in the present calculation ($T = 1.183$ s) corresponds to a resonance frequency of this sloshing motion.

3.2. 2-D sloshing in an oil tanker

In this section, 2-D sloshing motion of partially filled rectangular oil tanker is considered. Definition of the problem and the geometry are given in Figure 12(a). Density and viscosity of crude oil are $890\,\mathrm{kg/m^3}$ and 8×10^{-3} Pa.s, respectively. Gravity acts downward. The tanker is subjected to sinusoidal accelerations in horizontal (x) and vertical (y) directions as well as rotation about a specified axis (z). The motion of tanker is described as $D_x = A_x \sin(\omega_x t)$, $D_y = A_y \sin(\omega_y t)$ and $\theta_z = \Theta_z \sin(\omega_z t)$, where D and θ represent the linear and the angular displacements. A and Θ denote the linear and the angular amplitudes, respectively, and ω is the frequency. Subscripts x, y and z represent each co-ordinate directions. The parameters used to specify the motion are listed in Table I.

Calculations have been performed for two tankers; without and with a baffle. In the latter case, the baffle was assumed to be 13.5 m high and located at the centre of the bottom. For both cases, the origin of co-ordinate system is placed at 10 m above the bottom along the vertical centreline. Initially, crude oil is at rest and pressure is in hydrostatic equilibrium. Depth of oil, d, is 9 m. Frictionless boundaries were assumed between the fluid and the wall.

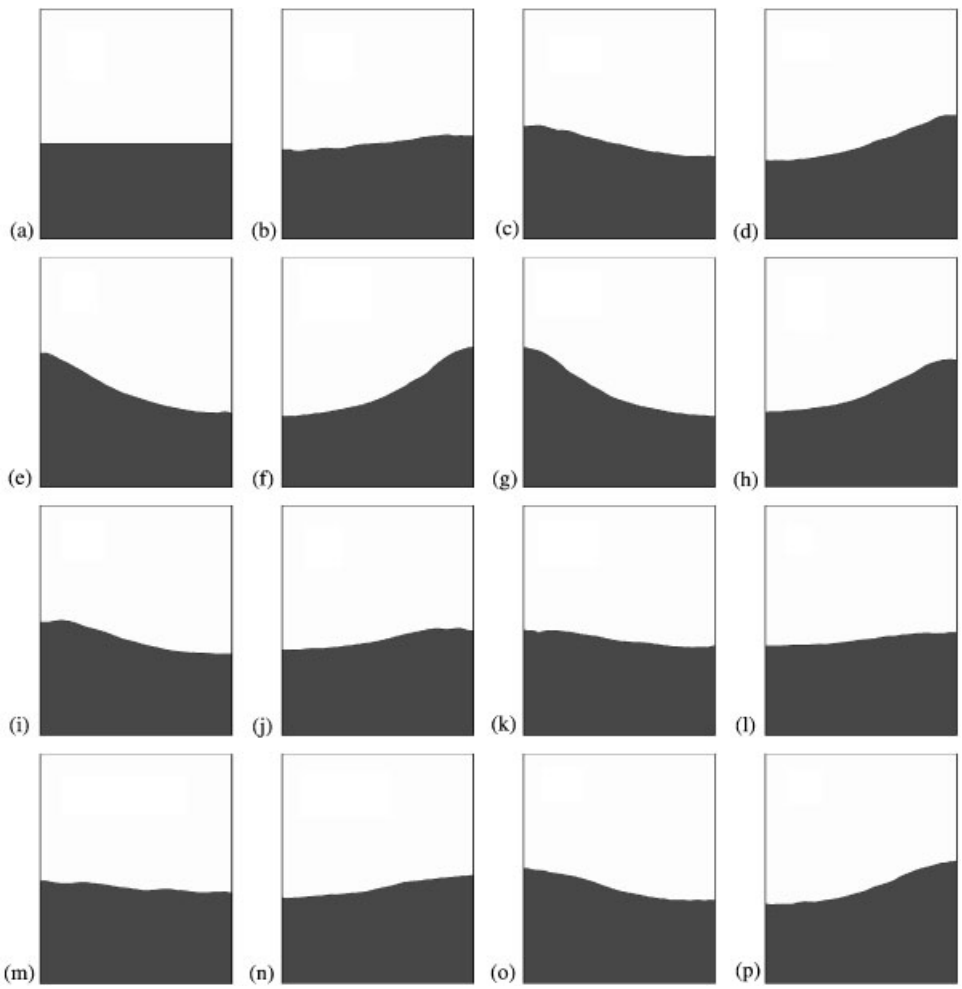

Figure 9. Free surface profiles in a container subject to forced sinusoidal horizontal oscillation ($A = 0.93$ cm, $\omega = 5.31$, $T = 1.183$ s). Results obtained with the present numerical scheme. Time increment for each figure is $\Delta t = 1.8$ s.

For the tanker without baffle, a larger number of grid points were used in the y-direction since vigorous sloshing motion was expected. The mesh used for the tanker without baffle consists of non-uniform 52×41 grids (see Figure 12(b)). The mesh used for the tanker with a baffle consists of non-uniform 52×31 grids (see Figure 12(c)).

Figure 13 shows the calculated free surface profiles in the tanker without baffle. The free surface wave travels from side to side and climbs higher up the vertical walls as time elapses. Fluid even splashes during collision with the ceiling of the tanker. A separated fluid fragment moves along the wall and then falls down. This seems to be in slight discrepancy with reality, where the fluid fragment is supposed to rebound from the wall. The inability to predict the rebound phenomenon is probably attributable to the boundary conditions specified on the wall,

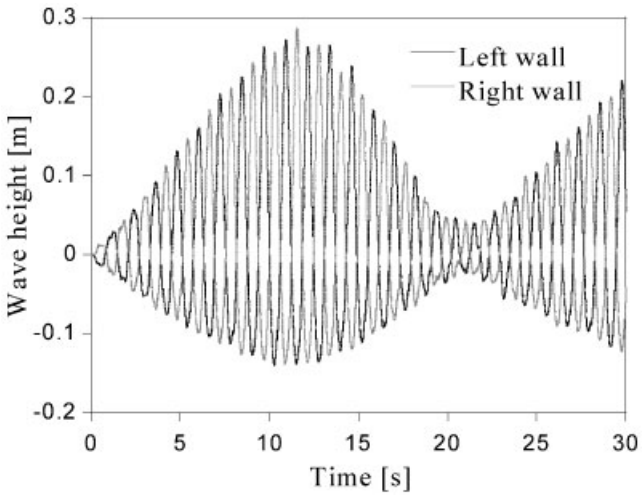

Figure 10. Wave heights at vertical walls as functions of time during sloshing in a container subject to forced sinusoidal horizontal oscillation ($A = 0.93$ cm, $\omega = 5.31$, $T = 1.183$ s). Results obtained with the present numerical scheme.

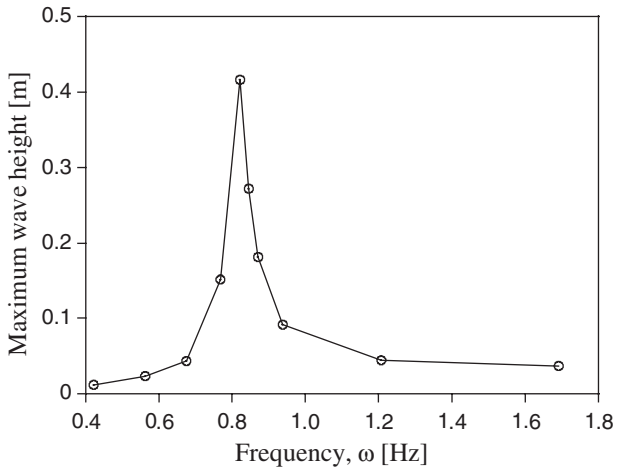

Figure 11. Maximum upward wave height at the left wall as a function of frequency in a container subject to forced sinusoidal horizontal oscillation. Results obtained with the present numerical scheme.

where normal velocity was assumed to be zero at all times. The sloshing motion becomes more and more amplified and eventually fluid starts to roll over in the whole tanker. In the tanker with a baffle, on the other hand, sloshing motion is restrained significantly by presence of the baffle as shown in Figure 14. The sloshing motion is confined within each region separated by the baffle. Comparison of above two cases shows that proper selection of baffle can minimize sloshing motion in partially filled containers.

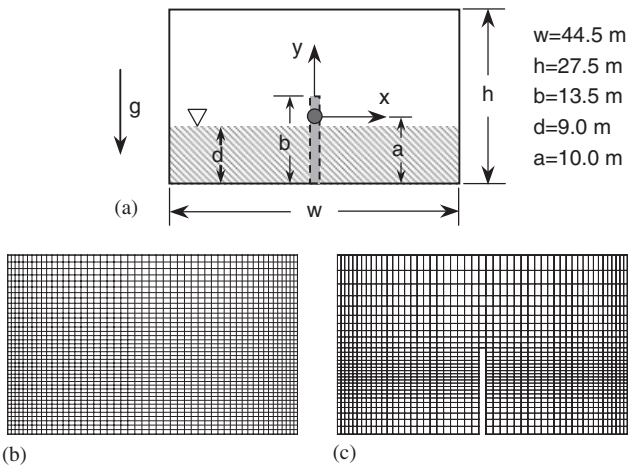

Figure 12. Definition sketch and numerical mesh systems for 2-D sloshing in an oil tanker. A baffle may be present at the centre of the bottom. (a) A tanker partially filled with crude oil, (b) mesh for the tanker without a baffle (52×41), and (c) mesh for the tanker with a baffle (52×31).

Table I. Parameters for 2-D sloshing motion.

	x	y	z
Amplitude (m or °)	2	5	15°
Period (s)	12.0	6.4	8.0
Frequency	0.524	0.982	0.785

When the height of baffle is lowered, the fluid on one side goes over the baffle to the other side. However, the present numerical algorithm failed to give accurate description of merging and splashing phenomena. This seems to be caused by the coarse grids used near the baffle, where a large amount of momentum is transported by a lump of fluid crossing the baffle. In addition, another possible reason might be an iterative nature adopted in the solution procedure of flow field, where the solution is obtained on the basis of local divergence in each element [2]. Therefore, dense grids should be prepared in the region where radical flow motion is expected. However, it is not possible to know in advance where such radical motion will take place. Moreover, such dense grids will increase the computation time significantly. A more reliable solution of problems associated with multiply connected fluid region should be further investigated.

3.3. 3-D sloshing in an oil tanker

In this section, 3-D sloshing motion of crude oil in a tanker is considered. A problem definition is given in Figure 15(a). The tanker is subject to sinusoidal accelerations with six degrees of freedom; three translational and three rotational motions. The motion of tanker is described as $D_x = A_x \sin(\omega_x t - \pi) + A_x \omega_x t$, $D_y = A_y \sin(\omega_y t)$, $D_z = A_z \sin(\omega_z t)$, $\theta_x = \Theta_x \sin(\omega_x t)$, $\theta_y = \Theta_y \sin(\omega_y t)$, and $\theta_z = \Theta_z \sin(\omega_z t)$. Subscripts x, y and z represent each co-ordinate

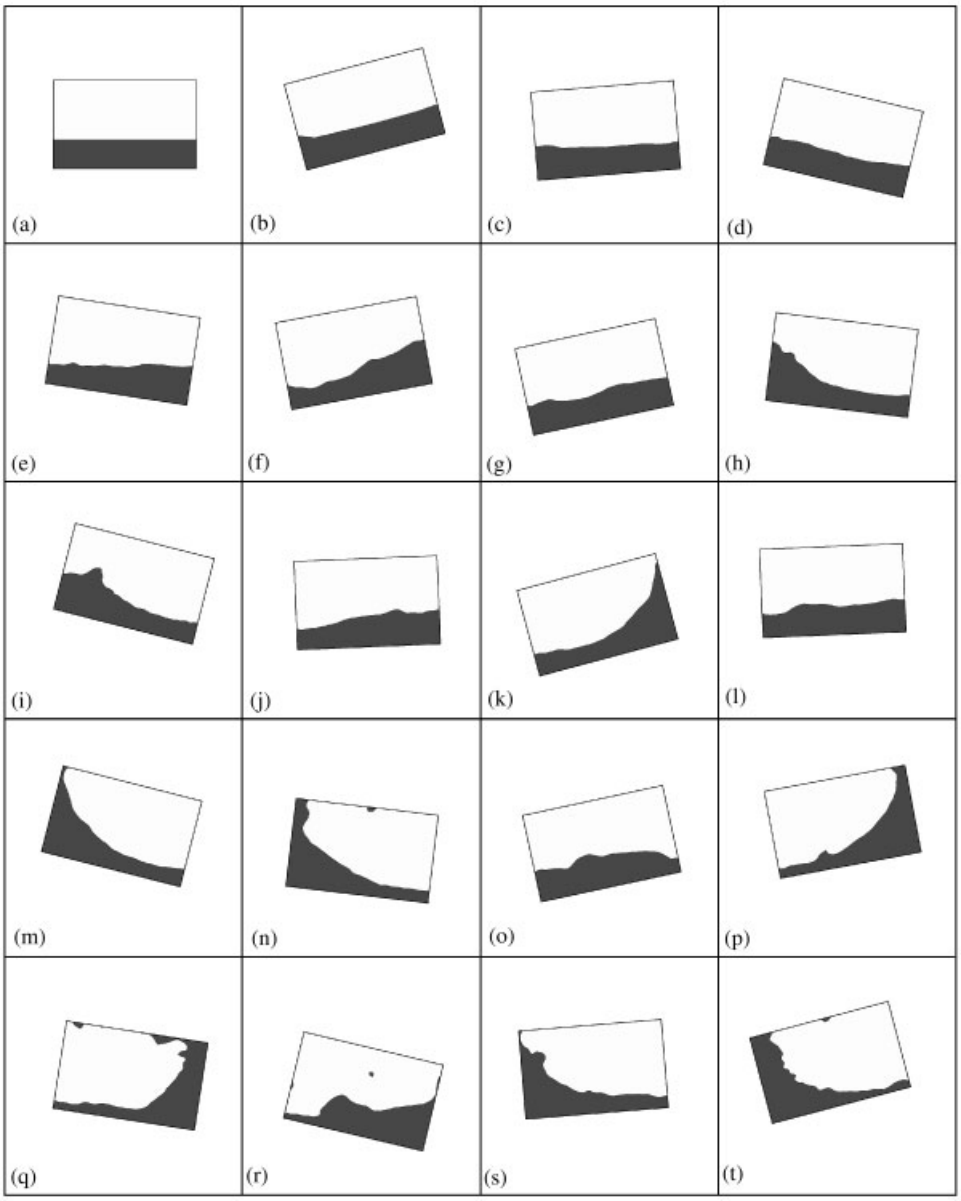

Figure 13. Free surface profiles of sloshing motion in the oil tanker without a baffle. Results obtained with the present numerical scheme. Time increment for each figure is $\Delta t = 1.8$ s.

direction. The tanker is assumed to advance in the positive x-direction with an average speed of 20 km/h. The parameters used to specify the motion are listed in Table II.

Calculation has been performed for a tanker without baffle. Tanker with a baffle was not considered since drastic sloshing motion was not expected. The origin of co-ordinate system

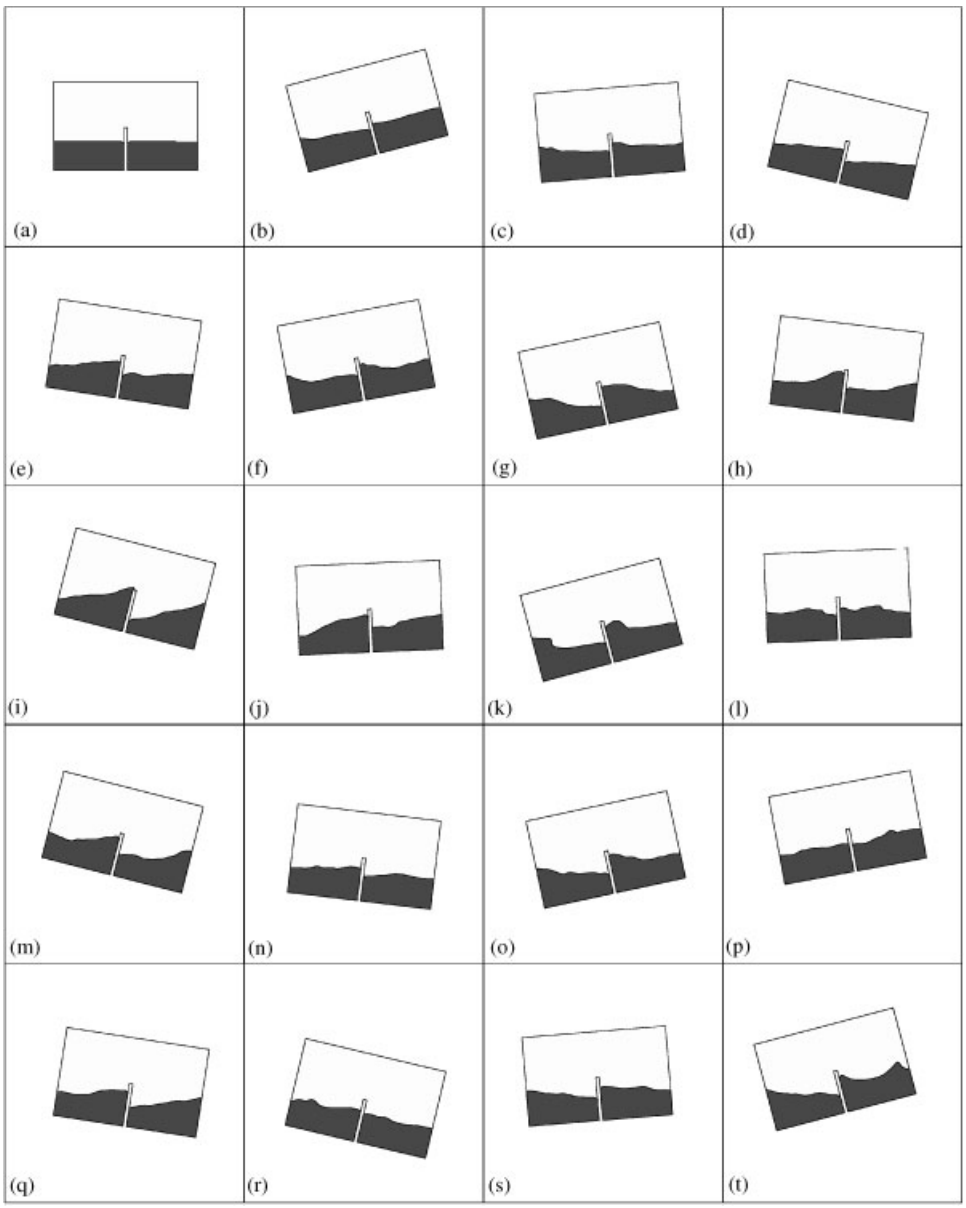

Figure 14. Free surface profiles of sloshing motion in the oil tanker with a baffle. Results obtained with the present numerical scheme. Time increment for each figure is $\Delta t = 1.8$ s.

is placed at 10 m above the bottom along the vertical centreline. Initially, crude oil is at rest and pressure is in hydrostatic equilibrium. Depth of oil, d, is 9 m. Frictionless boundaries were assumed between the fluid and the wall. The mesh consists of non-uniform $26 \times 21 \times 17$ grids, where the total numbers of nodes and finite elements are 9282 and 8000, respectively (see Figure 15(b)).

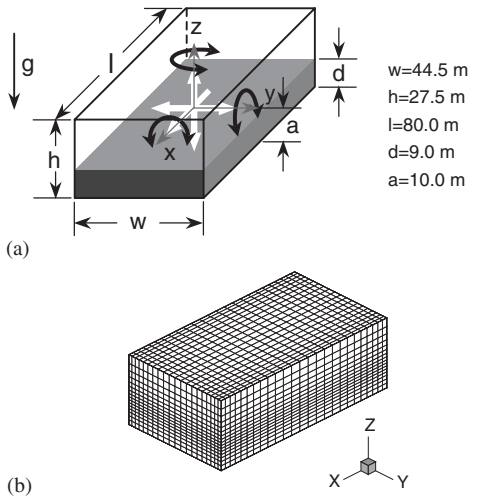

Figure 15. Definition sketch and numerical mesh system for 3-D sloshing in an oil tanker. (a) A tanker partially filled with crude oil and (b) non-uniform $26 \times 21 \times 17$ mesh.

Table II. Parameters for 3-D sloshing motion.

	Translation			Rotation		
	x	*y*	*z*	*x*	*y*	*z*
Amplitude (m or °)	53.05	2	4	8°	−5°	2°
Period (s)	60	14	9	8	10	12
Frequency	0.105	0.449	0.698	0.785	0.628	0.524

Calculation has been performed for initial 60 s. Figure 16 shows the calculated free surface profiles. Since rolling motion (rotation with respect to the *x*-axis) is predominant relative to other ones, the free surface wave almost travels from side to side. The wave climbs up higher as time elapses. In addition to translational accelerations, existence of rolling, pitching and yawing motions made a striking contrast in the run-up heights at each corner. This asymmetric sloshing motion of crude oil can produce an unexpected reaction force against the oil tanker. From the large amplitude sloshing motion observed in Figure 16, necessity of a baffle system and its design in the transportation facilities can be well understood again.

4. CONCLUDING REMARKS

A new VOF-based algorithm has been proposed in a separate article by the present authors for the transient free surface flow problems. The new free surface tracking scheme is characterized by two numerical tools; orientation vector and baby-cell. In this paper, the proposed numerical algorithm was applied to 2-D and 3-D cavity filling and sloshing problems. Excellent performance of the proposed numerical algorithm has been demonstrated through

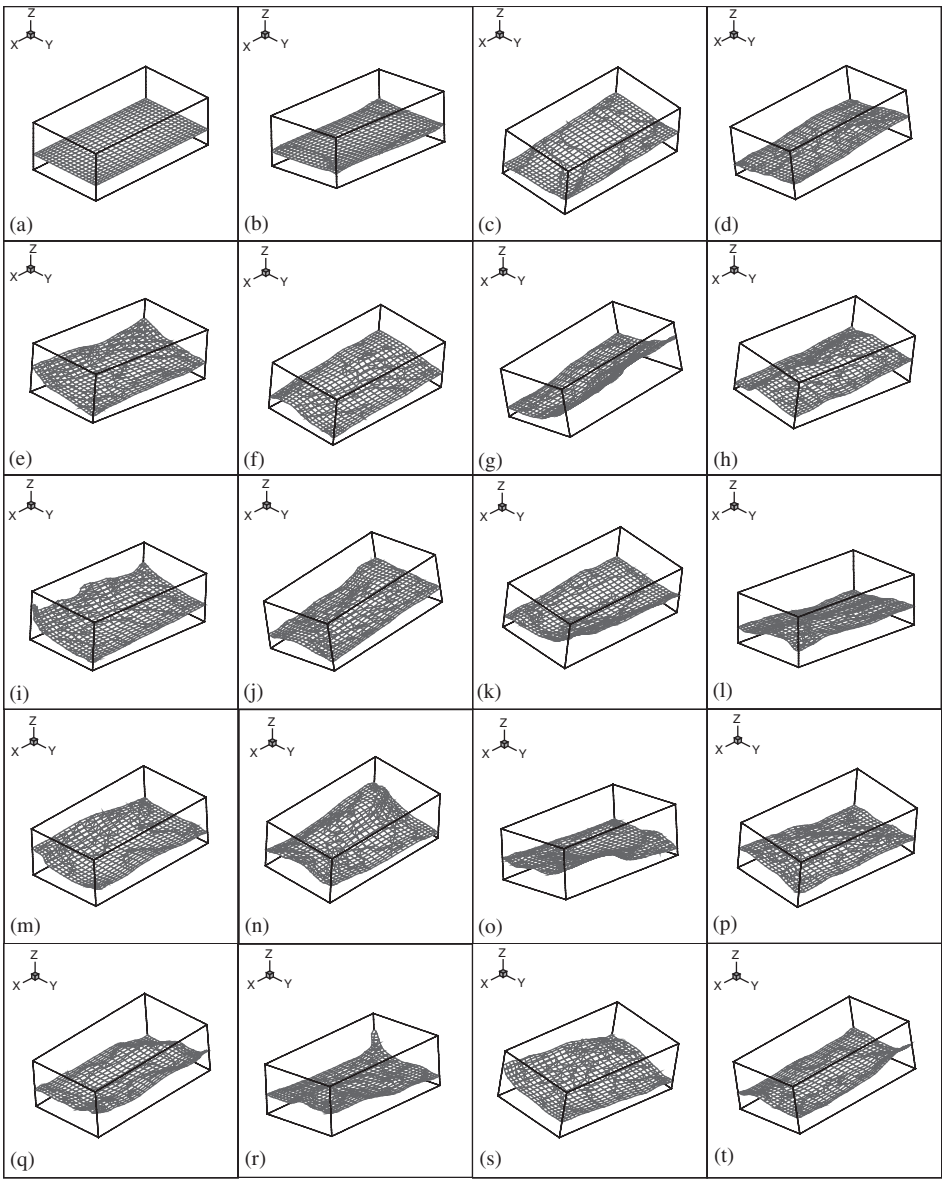

Figure 16. 3-D free surface profiles of sloshing motion in an oil tanker. Results obtained with the present numerical scheme. Time increment for each figure is $\Delta t = 3.0$ s.

numerical simulations. The calculated results have demonstrated applicability of the proposed numerical algorithm to the practical problems of large free surface motion. The present numerical algorithm resolved successfully the free surfaces interacting with each other. However, more improvement should be made for a reliable settlement of problems associated with wall boundary conditions in cavity filling analysis and multiply connected fluid region in sloshing

problems. Implementation of surface tension that plays an important role in small scale problems and analysis of thermal processes accompanying phase change remain to be further investigated.

NOMENCLATURE

A	linear amplitude
D	linear displacement
$\mathrm{d}A$	infinitesimal area element on the wall
$\mathrm{d}V$	infinitesimal volume element on the wall
f_i^t	equivalent body force per unit volume acting in the ith co-ordinate direction
L_c	characteristic length
Re	Reynolds number
T	period
t	time
$\bar{t}_i$	surface traction
u_i^w	ith component of tangential velocity on the wall
V_avg	average inlet velocity

Greek letters

δ	boundary layer thickness
μ	viscosity
Θ	angular amplitude
θ	angular displacement
ρ	density
ω	frequency

ACKNOWLEDGEMENTS

This work was supported by the Brain Korea-21 project and by Korea Ministry of Science and Technology through the National Lab Project.

REFERENCES

1. Hirt CW, Nichols BD. Volume of fluid (VOF) method for the dynamics of free boundaries. *Journal of Computational Physics* 1981; **39**:201–225.
2. Kim MS, Lee WI. A new VOF-based numerical scheme for the simulation of fluid flow with free surface. Part I: new free surface-tracking algorithm and its verification. *International Journal for Numerical Methods in Fluids* 2003; **42**:765–790.
3. Kim MS. Finite element study of fluid flow with moving free surface. *Ph.D. Thesis*, Seoul National University; 1998.
4. Dhatt G, Gao DM, Cheikh AB. A finite element simulation of metal flow in moulds. *International Journal for Numerical Methods in Engineering* 1990; **30**:821–831.
5. Chan KS, Pericleous K, Cross M. Numerical simulation of flows encountered during mold-filling. *Applied Mathematical Modelling* 1991; **15**:624–631.
6. Minaie B, Stelson KA, Voller VR. Analysis of flow patterns and solidification phenomena in the die casting process. *Journal of Engineering Materials Technology* 1991; **113**:296–302.

7. Usmani AS, Cross JT, Lewis RW. A finite element model for the simulations of mould filling in metal casting and the associated heat transfer. *International Journal for Numerical Methods in Engineering* 1992; **35**: 787–806.
8. Rice AB. Numerical simulation of mold filling processes. *Ph.D. Thesis*, Purdue University; 1993.
9. Lewis RW, Usmani AS, Cross JT. Efficient mould filling simulation in castings by an explicit finite element method. *International Journal for Numerical Methods in Fluids* 1995; **20**:493–506.
10. Hetu JF, Ilinica F. A finite element method for casting simulations. *Numerical Heat Transfer Part A* 1999; **36**:657–679.
11. Gao DM. A Three-dimensional hybrid finite element-volume tracking model for mould filling in casting processes. *International Journal for Numerical Methods in Fluids* 1999; **29**:877–895.
12. Goldschmit MB, Principe RJ, Koslowski M. Applications of A (k–ε) model for the analysis of continuous casting processes. *International Journal for Numerical Methods in Engineering* 1999; **46**:1505–1519.
13. Gaston L, Kamara A, Bellet M. An arbitrary Lagrangian–Eulerian finite element approach to non-steady state turbulent fluid flow with application to mould filling in casting. *International Journal for Numerical Methods in Fluids* 2000; **34**:341–369.
14. Swaminathan CR, Voller VR. A time-implicit filling algorithm. *Applied Mathematical Modelling* 1994; **18**: 101–108.
15. Shin S, Lee WI. Finite element analysis of incompressible viscous flow with moving free surface by selective volume of fluid method. *International Journal of Heat and Fluid Flow* 2000; **21**:197–206.
16. Ramaswamy B, Kawahara M, Nakayama T. Lagrangian finite element method for the analysis of two-dimensional sloshing problems. *International Journal for Numerical Methods in Fluids* 1986; **6**:659–670.
17. Okamoto T, Kawahara M. Two-dimensional sloshing analysis by Lagrangian finite element method. *International Journal for Numerical Methods in Fluids* 1990; **11**:453–477.
18. Ramaswamy B, Kawahara M. Arbitrary Lagrangian–Eulerian finite element method for unsteady, convective, incompressible viscous free surface fluid flow. *International Journal for Numerical Methods in Fluids* 1987; **7**:1053–1075.
19. Huerta A, Liu WK. Viscous flow with large free surface motion. *Computer Methods in Applied Mechanics and Engineering* 1988; **69**:277–324.
20. Partom IS. Application of the VOF method to the sloshing of a fluid in a partially filled cylindrical container. *International Journal for Numerical Methods in Fluids* 1987; **7**:535–550.
21. Jun L, Spalding DB. Numerical simulation of flows with moving interfaces. *PhysicoChemical Hydrodynamics* 1988; **10**:625–637.
22. Kothe DB, Mjolsness RC, Torrey MD. RIPPLE: A computer program for incompressible flows with free surfaces. *Los Alamos National Laboratory Report*, LA-12007-MS. 1994.
23. Schlichting H. *Boundary Layer Theory*. McGraw-Hill: New York, 1979.
24. White FM. *Fluid Mechanics*. McGraw-Hill: New York, 1988.

